Cell Reports

A Hallucinogenic Serotonin-2A Receptor Agonist Reduces Visual Response Gain and Alters Temporal Dynamics in Mouse V1

Graphical Abstract

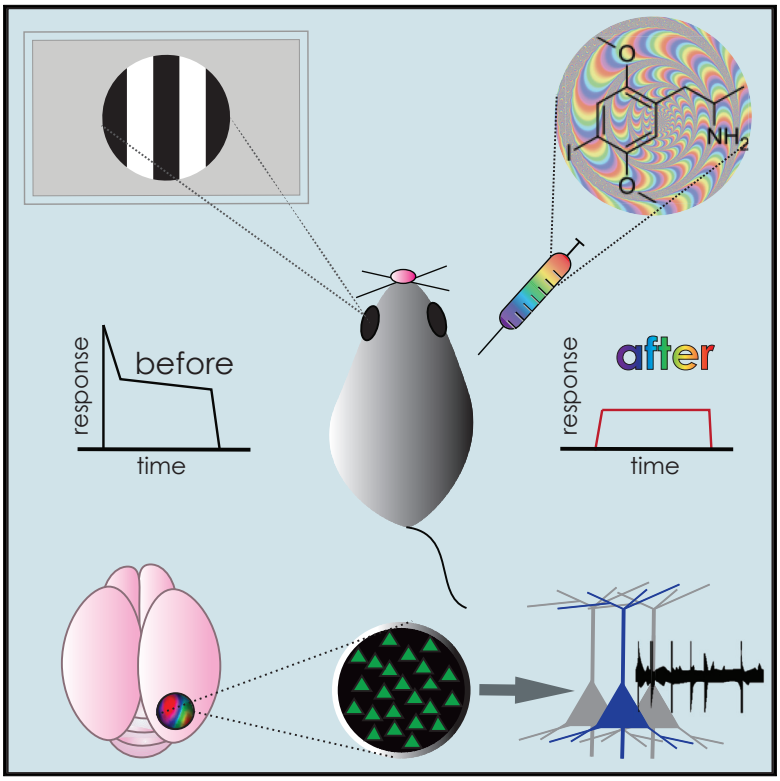

Highlights

- The 5-HT_{2A} R agonist DOI reduces sensory drive in mouse V1
- DOI exerts layer and cell-type specific effects on temporal processing
- DOI alters contextual modulation by reducing surround suppression
- The results support models of hallucination involving reduced bottom-up sensory drive

Authors

Angie M. Michaiel, Philip R.L. Parker, Cristopher M. Niell

Correspondence

cniell@uoregon.edu

In Brief

Activation of serotonin-2A receptors (5-HT_{2A}Rs) is associated with hallucinations, but impacts on sensory processing are largely unknown. Michaiel et al. demonstrate that the 5-HT_{2A}R agonist DOI strongly reduces sensory-evoked activity and disrupts temporal dynamics. These results support models of hallucinations that propose reduced bottom-up sensory drive.

Michaiel et al., 2019, Cell Reports *26*, 3475–3483
March 26, 2019
https://doi.org/10.1016/j.celrep.2019.02.104

CellPress

Cell Reports
Report

A Hallucinogenic Serotonin-2A Receptor Agonist Reduces Visual Response Gain and Alters Temporal Dynamics in Mouse V1

Angie M. Michaiel,[1,2] Philip R.L. Parker,[1,2] and Cristopher M. Niell[1,3,*]
[1]Institute of Neuroscience and Department of Biology, University of Oregon, Eugene, OR 97403, USA
[2]These authors contributed equally
[3]Lead Contact
*Correspondence: cniell@uoregon.edu
https://doi.org/10.1016/j.celrep.2019.02.104

SUMMARY

Sensory perception arises from the integration of externally and internally driven representations of the world. Disrupted balance of these representations can lead to perceptual deficits and hallucinations. The serotonin-2A receptor (5-HT_{2A}R) is associated with such perceptual alterations, both in its role in schizophrenia and in the action of hallucinogenic drugs. Despite this powerful influence on perception, relatively little is known about how serotonergic hallucinogens influence sensory processing in the neocortex. Using widefield and two-photon calcium imaging and single-unit electrophysiology in awake mice, we find that administration of the hallucinogenic selective 5-HT_{2A}R agonist DOI (2,5-dimethoxy-4-iodoamphetamine) leads to a net reduction in visual response amplitude and surround suppression in primary visual cortex, as well as disrupted temporal dynamics. However, basic retinotopic organization, tuning properties, and receptive field structure remain intact. Our results provide support for models of hallucinations in which reduced bottom-up sensory drive is a key factor leading to altered perception.

INTRODUCTION

Both externally (bottom-up) and internally (top-down) driven representations of the world contribute to sensory perception. Disruption of accurate sensory perception, as occurs during hallucination, is hypothesized to result from increased top-down and/or decreased bottom-up signaling, leading to excessive reliance on prediction at the expense of sensory input (Cassidy et al., 2018; Grossberg 2000). Abnormal serotonin-2A receptor (5-HT_{2A}R) activity is implicated in sensory hallucination, defined as the misinterpretation of sensory stimuli in space or time or the perception of an absent external stimulus. In particular, hallucinations and altered perception resulting from both schizophrenia and psychedelic drug administration are prevented by antagonism of 5-HT_{2A}Rs, supporting a central role of this receptor in mediating hallucinations (Schmidt et al., 1995; Vollenweider et al., 1998).

The cognitive and perceptual effects of 5-HT_{2A}R modulation have been extensively studied, particularly in the context of psychedelic drugs (reviewed in Nichols, 2016). Recent studies have begun to elucidate the action of serotonergic hallucinogens on large-scale brain activity in humans using neuroimaging methods (Preller et al., 2018; Carhart-Harris et al., 2016). However, the impact on sensory information processing at the level of single neurons and populations of neurons is largely unknown. To our knowledge, measures of visually evoked responses after 5-HT_{2A}R agonist administration in humans are limited to one study, which showed large reductions in pre-stimulus alpha-band LFP synchronization (Kometer et al., 2013). There have been few studies of individual V1 neuron responses to visual stimuli following administration of 5-HT_{2A}R agonists, yielding varying findings of suppression, facilitation, or bidirectional changes in firing rate (Rose and Horn, 1977; Fox and Dray, 1979; Dray et al., 1980; Watakabe et al., 2009). Furthermore, these studies were conducted in anesthetized animals, did not measure individual neuron-tuning properties, and did not address cell type or layer specificity.

The selective 5-HT_{2A}R agonist DOI (2,5-dimethoxy-4-iodoamphetamine) is known to be a powerful hallucinogen in humans (Shulgin and Shulgin, 1991) and has been used extensively to study 5-HT_{2A}R function in animal models, particularly of schizophrenia and psychedelic drug action (for reviews, see Hanks and González-Maeso, 2013; Nichols 2016). In this study, we assessed the impact of DOI on visual processing at multiple scales, from retinotopic maps to individual neurons, using widefield and two-photon calcium imaging and single-unit electrophysiology in awake, head-fixed mice. Our results demonstrating how a serotonergic hallucinogen disrupts sensory processing should provide a deeper understanding of how cortical circuits generate a representation of the world based on sensory input.

RESULTS

To measure the effects of 5-HT_{2A}R activation on spatial and temporal processing in visual cortex, we measured visual responses in mice head-fixed on a spherical treadmill (Dombeck et al., 2007) using widefield imaging and two-photon calcium imaging, and single-unit electrophysiology with silicon probes (Figure 1A).

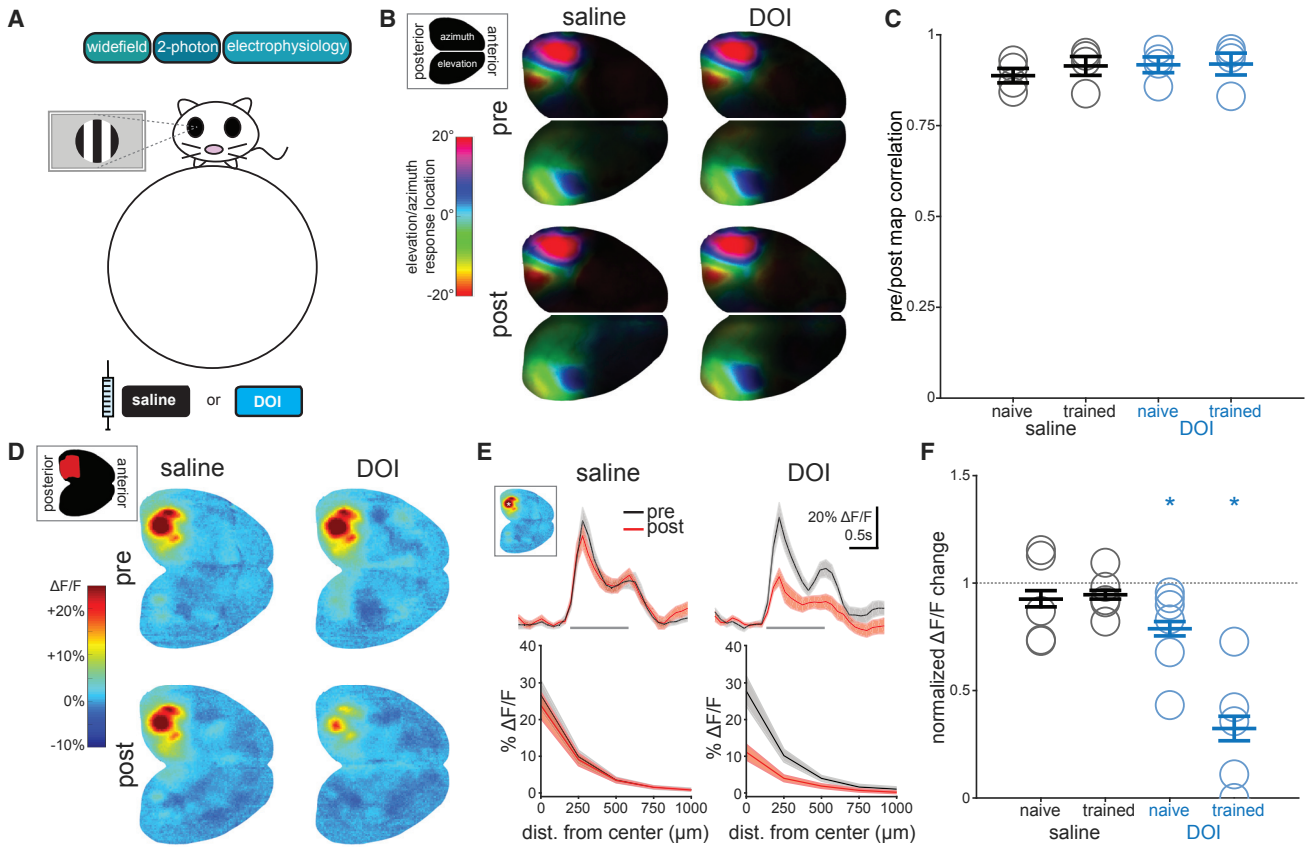

Figure 1. DOI Reduces Visually Evoked Responses in Visual Cortex

(A) In all experiments, we measured responses to visual stimuli before and 20 min after drug administration using widefield and two-photon GCaMP6s imaging or silicon probe electrophysiology in awake, head-fixed mice on a spherical treadmill.

(B) Group-averaged phase maps from widefield responses to bilateral stimulus presentation moving along the azimuth (left hemispheres) or elevation (right hemispheres) before and after drug administration.

(C) Correlation coefficients for pre- versus post-phase maps across groups. Circles represent individual animals, and bars represent mean ± SEM.

(D) Widefield responses to grating patches presented to the right eye before and after drug administration during stationary periods. Inset shows cortical schematic with left visual areas in red.

(E) Cycle averages (top; gray bars represent stimulus period) and spatial spread of response (bottom) measured from a manually selected point in V1 (white asterisk, inset).

(F) Changes to visually evoked responses after drug administration across groups. Open circles represent individual animals, bars are mean ± SEM. A value of 1 represents no change, asterisks indicate significant change ($p < 0.05$; saline naive: n = 5; saline trained: n = 5; DOI naive: n = 6; DOI trained: n = 5).

Following presentation of a set of visual stimuli, mice received a subcutaneous injection of either saline (control) or the 5-HT_{2A}R agonist DOI (10 mg/kg; see STAR Methods and Figure S1 for an explanation of dose choice), and after a 15- to 20-min waiting period, the stimulus set was repeated. To explore how previous experience with visual stimuli may influence effects of 5-HT_{2A}R signaling, we performed a subset of these passive viewing experiments with animals previously trained on a visually guided task, in addition to standard non-trained animals. As visual responses and surround suppression are modulated by behavioral state (Niell and Stryker, 2010; Ayaz et al., 2013), we separated data into stationary or running periods for statistical comparison. Notably, neither pupil size nor fraction of time running was different following drug administration (Figure S2), suggesting that changes observed were not due to differences in behavioral state.

Widefield imaging of cortical excitatory neurons in CaMKIIa-tTA:tetO-GCaMP6s mice (GCaMP6s mice; Wekselblatt et al., 2016) revealed no change in the retinotopic map of azimuth and elevation in visual cortex (Figures 1B and 1C; $p = 0.999$, Kruskal-Wallis; see also Movie S1) but a dramatic reduction in responses to grating patches in visual areas after DOI, but not saline, administration during stationary periods (Figures 1D and 1E). Interestingly, this reduction was larger in animals that had previously received training on a visual task than in animals naive to training (Figure 1F; $p = 0.012$, Kruskal-Wallis; paired t test: DOI trained: $p = 0.031$, $n = 5$; DOI naive: $p = 0.049$, $n = 6$; saline trained: $p = 0.192$, $n = 5$, saline naive: $p = 0.917$, $n = 5$). Passive stimuli used here were similar to those used in previous behavioral experiments (circular grating patches) but were different in size and location in visual space (see STAR Methods for further details), arguing against effects of perceptual learning. Furthermore,

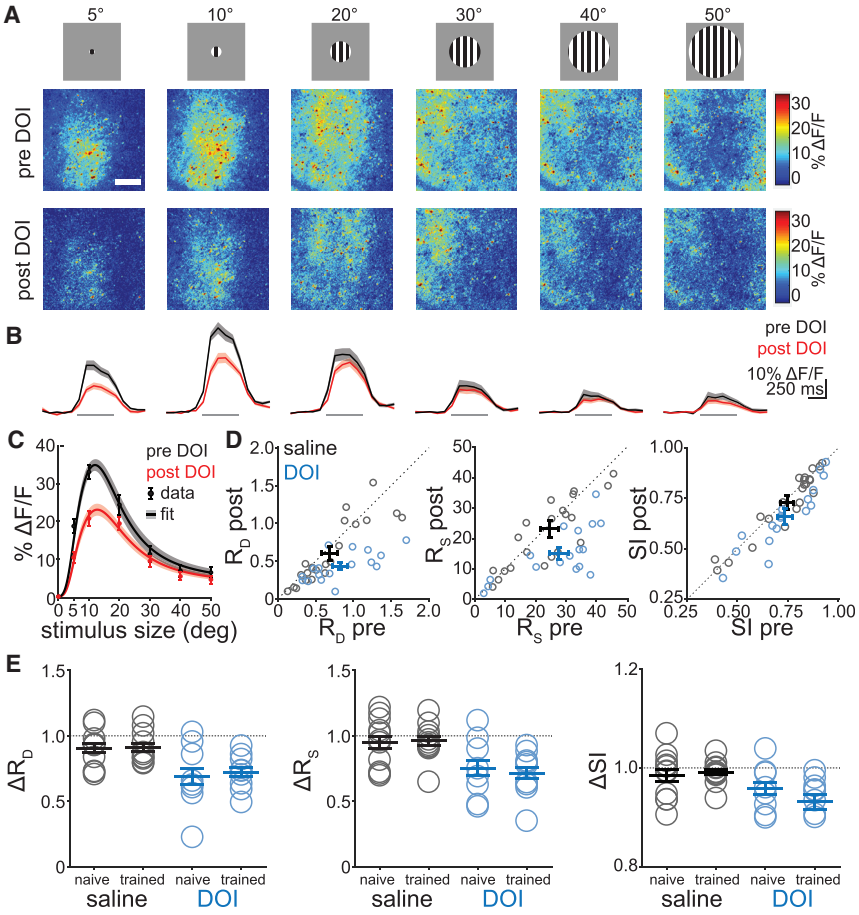

Figure 2. DOI Reduces Surround Suppression in V1 L2/3 Excitatory Neurons

(A) Two-photon images in V1 showing responses to stimuli of increasing size before (top) and after (bottom) DOI administration in an example animal. Note surround suppression in the neuropil response. White scale bar in the top left image represents 200 μm. Data are from stationary periods only (see text for running data).

(B) Cycle averages of extracted (see STAR Methods) individual L2/3 excitatory neurons to corresponding stimuli shown above (gray bars show stimulus period), averaged within then across animals before (black) and after (red) DOI administration.

(C) Size tuning curve from data in (B) showing average responses of individual neurons with increasing stimulus size. Data are presented as points with error bars, and divisive normalization fits are shown as lines with shaded error bars.

(D) Driving (R_D) and suppressive (R_S) field coefficients and suppression index (SI) from divisive normalization fits of individual animal size-tuning curves for saline (black) and DOI (blue) before and after drug administration.

(E) Changes in driving and suppressive field coefficients and SI within each group before and after drug administration. A value of 1 represents no change, and asterisks indicate a significant change ($p < 0.025$ for R_D, R_S; $p < 0.05$ for SI; n = animals/cells: saline naive: n = 11/269; saline trained: n = 11/144; DOI naive: n = 8/144; DOI trained: n = 9/215).

baseline responses between trained and naive animals were not statistically different (Figure S3).

Given that widefield signals represent the summed activity in cell bodies, dendrites, and axons from many different excitatory cortical neurons, we next used two-photon calcium imaging to study the effect at the level of individual neurons, focusing on spatial integration. A key mechanism by which V1 neurons integrate information across space is through surround suppression, where larger stimuli tend to decrease V1 responses. This phenomenon can be explained by divisive normalization of "driving" classical receptive field (CRF) responses by "suppressive" responses in the extra-CRF (eCRF). We performed two-photon imaging in L2/3 of V1 in GCaMP6s mice while showing grating patches of varying sizes (5°–50°), which revealed clear surround suppression in the neuropil responses (Figure 2A; see also Movie S2). Consistent with widefield imaging, DOI reduced the magnitude of visual responses at the level of neuropil, as well as the visual responses of individual neurons (Figure 2B). We computed size tuning curves from the individual neuron data (Figure 2C), fit these with a divisive normalization model (Ayaz et al., 2013; see STAR Methods), and measured the coefficients of the driving (R_D) and suppressive (R_S) fields. Both R_D and R_S were reduced after administration of DOI, but not saline (Figure 2D). These DOI-induced changes in R_D and R_S were significant for both naive and trained animals during stationary periods (Figure 2E; R_D p = 0.021, R_S p = 0.010, Kruskal-Wallis; paired t test: DOI trained: R_D p = 0.003, R_S p = 0.002 n = 9/215; DOI naive: R_D p = 0.020, R_S p = 0.012, n = 8/144; saline trained: R_D p = 0.201, R_S p = 0.730 n = 11/197; saline naive: R_D p = 0.159, R_S p = 0.317, n = 11/269; where n = animals/cells; alpha = 0.025 corrected for multiple comparisons). DOI also reduced R_D during running bouts in trained, but not naive animals (not shown; R_D p = 0.023, R_S p = 0.032, Kruskal-Wallis; paired t test: DOI trained: R_D p = 0.015, R_S p = 0.026; DOI naive: R_D p = 0.084, R_S p = 0.357; saline trained: R_D p = 0.773, R_S p = 0.031; saline naive: R_D p = 0.744, R_S p = 0.559; alpha = 0.025 corrected for multiple comparisons). Consistent with these changes in R_D and R_S, DOI reduced the suppression index in naive (stationary only) and trained (stationary and running) animals (Figures 2D and 2E; suppression index paired t test before versus after: DOI trained: p_{stat} = 0.005, p_{run} = 0.014; DOI naive: p_{stat} = 0.034, p_{run} = 0.814; saline trained: p_{stat} = 0.285, p_{run} = 0.150; saline naive: p_{stat} = 0.261, p_{run} = 0.390).

In order to determine how 5-HT_{2A}R activation affects temporal dynamics of population activity, we recorded local field potentials (LFPs) using silicon probes and found the average LFP power in all cortical layers was reduced across a wide frequency range following administration of DOI in both spontaneous (not shown) and visually evoked activity (Figure 3A; paired t test, corrected for multiple comparisons: stationary saline: p_{delta} = 0.184, p_{theta} = 0.531, p_{alpha} = 0.254, p_{beta} = 0.065, p_{gamma} = 0.0361,

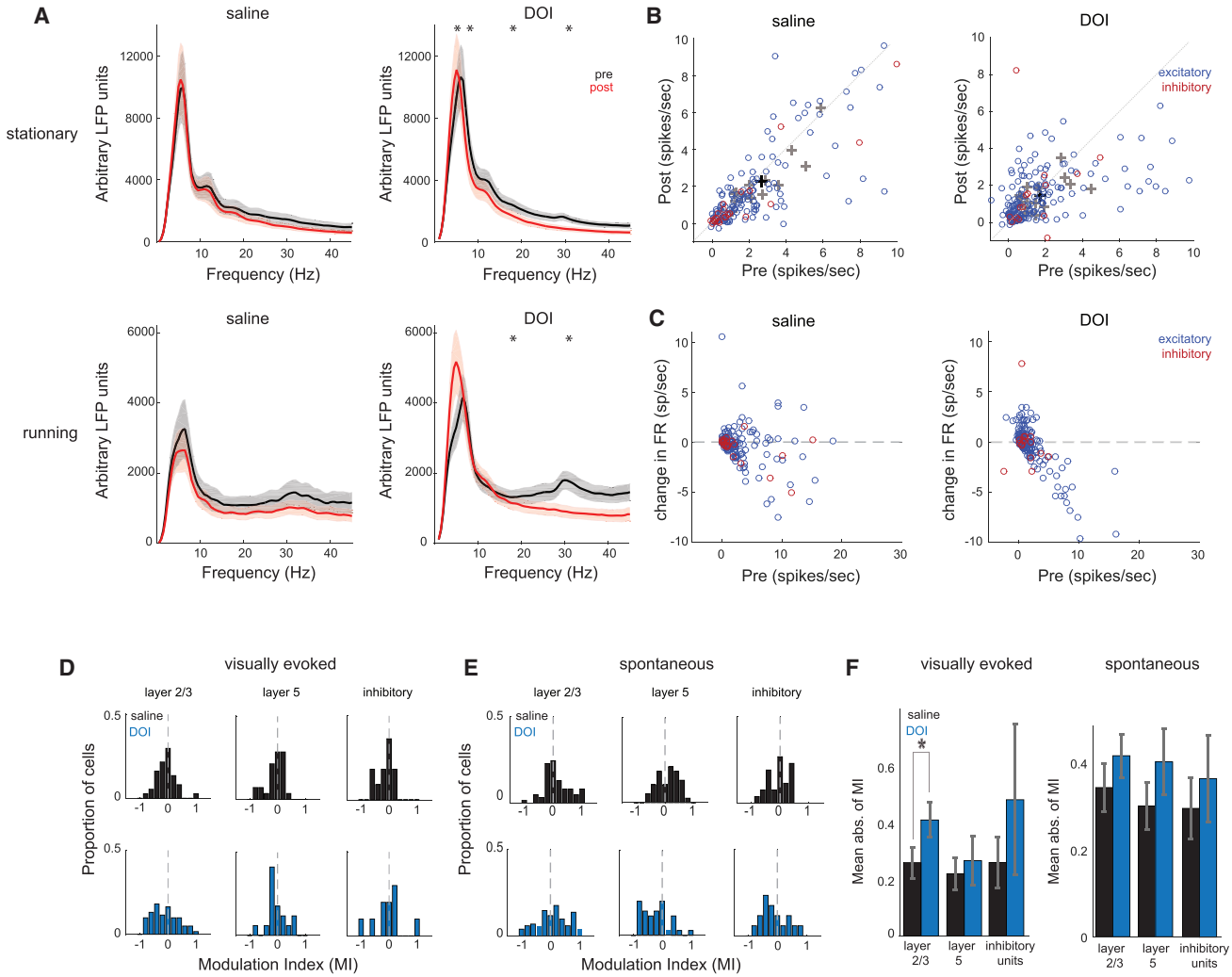

Figure 3. DOI Reduces LFP Power and Bidirectionally Modulates Visually Evoked Firing Rate

(A) Average stationary and running LFP power ± SEM before (black) and after (red) administration of saline or DOI in response to sinusoidal drifting gratings (n_{saline} = 12 sessions, n_{DOI} = 12 sessions).

(B) Peak visually evoked firing rate before or after saline or DOI during stationary periods. Blue circles represent excitatory units, and red circles represent inhibitory units. 8% of saline units and 3% of DOI units are not shown. Black and gray crosses represent averages of all units and individual animals, respectively, including those not shown ($n_{saline\ exc}$ = 155 cells, $n_{saline\ inh}$ = 26 cells, n_{saline} = 15 animals, $n_{DOI\ exc}$ = 187 cells, $n_{DOI\ inh}$ = 17 cells, n_{DOI} = 15 animals).

(C) Change in peak firing rate as a function of initial peak firing rate. One saline and one DOI unit are not shown.

(D) Modulation indices (MIs) calculated from change in visually evoked peak firing rate between pre- and post-blocks. MI of 1 represents complete facilitation of firing rate after drug injection.

(E) MI distributions for spontaneous rates.

(F) Mean absolute value of MIs shows layer-specific changes between saline and DOI for the L2/3 evoked rate.

n = 12 animals; stationary DOI: p_{delta} = 0.127, p_{theta} = 0.0015, p_{alpha} = 0.002, p_{beta} = 0.0001, p_{gamma} = 0.0001, n = 12 animals; running saline: p_{delta} = 0.072, p_{theta} = 0.995, p_{alpha} = 0.572, p_{beta} = 0.616, p_{gamma} = 0.287, n = 12 animals; running DOI: p_{delta} = 0.766, p_{theta} = 0.0077, p_{alpha} = 0.02, p_{beta} = 0.0003, p_{gamma} = 0.0005, n = 12 animals; alpha = 0.01). Interestingly, the visual stimulus-evoked increase in gamma power (28–35 Hz) was completely abolished after DOI administration. These results are consistent with findings from studies of hallucinogenic drug effects in humans using electroencephalography (EEG) and magnetoencephalography (MEG) (Kometer et al., 2013; Carhart-Harris et al., 2016), which also show an overall reduction in oscillatory synchronization.

We next aimed to examine how individual V1 neuron activity is affected by 5-HT_{2A}R activation by analyzing responses of isolated single units to drifting sinusoidal gratings. We focused this analysis on L2/3 and L5 because they display distinct response properties (Niell and Stryker, 2008), and both excitatory and inhibitory neurons in these layers contain the highest 5-HT_{2A}R density in mouse neocortex (Weber and Andrade, 2010). Units were classified as putative excitatory or narrow-spiking inhibitory based on spike waveform (Niell and Stryker,

2008). As such, inhibitory neurons in this study are likely fast-spiking parvalbumin (PV) cells and not somatostatin (SOM)-expressing cells. Following DOI administration, the peak visually evoked firing rate of excitatory V1 neurons was bidirectionally modulated (Figure 3B; saline: r^2 = 0.74, p = 0.679, n = 155; DOI: r^2 = 0.44, p = 0.181, n = 187; paired t test). Interestingly, we observed rate-specific modulation of responses; neurons with initially low firing rates were facilitated, and neurons with initially high firing rates were suppressed (Figure 3C), similar to observations with 5-HT_{2A}R activation in anesthetized non-human primate and cat V1 (Watakabe et al., 2009; Rose and Horn, 1977). In contrast to the excitatory neuron population, inhibitory neurons did not change their peak evoked firing rate (saline: r^2 = 0.73, p = 0.103, n = 26; DOI: r^2 = 0.93, p = 0.812, n = 17; paired t test). The same pattern was observed during locomotive states (not shown; saline excitatory: r^2 = 0.55, p = 0.057, inhibitory: r^2 = 0.75, p = 0.215; DOI excitatory: r^2 = 0.44, p = 0.7.15e-05, inhibitory r^2 = 0.93, p = 0.577; paired t test).

To determine how strongly each cortical layer was affected by DOI, we calculated modulation indices of stationary peak firing rate across the neural population, where negative (positive) values represent neurons that reduced (increased) their rate following drug administration (Figures 3C and 3D). The distributions were shifted overall toward suppression; however, because these distributions were bidirectional, we calculated the mean absolute value for each layer to determine the strength of modulation independent of sign. This revealed visually evoked responses in L2/3 were more affected by DOI than saline (t test: p = 0.005, corrected for multiple comparisons), whereas spontaneous rate was not affected (Figure 3E). Thus, the effects of DOI are specific for layer and cell type and differ for spontaneous versus evoked activity.

We next determined how DOI affected the time course of V1 responses based on the peristimulus time histogram (PSTH) of responses to drifting gratings (Figure 4A). Following DOI administration, we saw layer-specific changes in the mean PSTH of visually responsive cells (neurons with peak visually evoked rate greater than 2 Hz in either the pre- or post-recording block). The mean response of both L2/3 and L5 was significantly reduced (two-sample Kolmogorov-Smirnov test; L2/3: p_{stat} = 0.0001, n = 37, p_{run} = 0.004, n = 61; L5: p_{stat} = 0.001, n = 13, p_{run} = 0.026, n = 19), consistent with more neurons being suppressed than enhanced, whereas inhibitory units were not affected (inhibitory [inh.]: p_{stat} = 0.878, n = 7, p_{run} = 0.878, n = 10).

The time course of the mean PSTH showed a transient response at stimulus onset followed by a smaller sustained response, which was most pronounced in L2/3 neurons (Figure 4A). Notably, the transient (first 500 ms after stimulus onset) and sustained (500 ms preceding stimulus offset) components were differentially affected by DOI. We separated the two temporal components and found that L2/3 was strongly suppressed during the transient component (p_{stat} = 0.0002, p_{run} = 0.0035) and was only affected during the sustained component when animals were running (p = 0.0007; Figure 4B). L5 and inhibitory units, in contrast, did not show a significant net change in either temporal component ($L5_{trans}$ p_{stat} = 0.0471; $L5_{trans}$ p_{run} = 0.864; $L5_{sus}$ p_{stat} = 0.436; $L5_{sus}$ p_{run} = 0.727; inh_{trans} p_{stat} = 0.587; inh_{trans} p_{run} = 0.875; inh_{sus} p_{stat} = 0.964; inh_{sus} p_{run} = 0.852). Thus, DOI administration disrupts temporal dynamics of visual responses in L2/3 by strongly reducing the onset transient.

We next determined if DOI affected the encoding of low-level stimulus features and feature selectivity. Across the recorded population of neurons, we found no change for the preferred grating orientation following DOI administration (Figure 4C; saline: r^2 = 0.92, p = 0.346, n = 37; DOI: r^2 = 0.87, p = 0.639, n = 33; not shown; saline running: r^2 = 0.87, p = 0.425, n = 27; DOI running: r^2 = 0.81, p = 0.873, n = 43; paired t test). The mean orientation selectivity index was also unaffected by DOI and saline administration (Figure 4D; Wilcoxon rank sum test on mean of stationary and running; saline: p = 0.362, n = 100; DOI: p = 0.214, n = 91). Preferred direction of grating motion and mean direction selectivity index (DSI) were also unchanged (not shown; Wilcoxon rank sum test; preferred direction saline stationary: r^2 = 0.95 p = 0.912 n = 33, running: r^2 = 0.5 p = 0.929 n = 25; DOI stationary: r^2 = 0.57 p = 0.861 n = 56; running: r^2 = 0.46 p = 0.486 n = 62; DSI saline stationary: p = 0.95 n = 71; running: p = 0.25 n = 71; DOI stationary: p = 0.33, n = 64; running: p = 0.70, n = 64). We also found no change in the distribution of spatial frequency preference for responsive cells, as the same proportions were selective to either low (0.01–0.02 cycles per degree [cpd]; paired t test mean of running and stationary; saline: p = 0.435; DOI: p = 0.823), medium (0.04–0.08 cpd; saline: p = 0.334; DOI: p = 0.397), or high (0.16–0.32 cpd; saline: p = 0.640; DOI: p = 0.485) spatial frequencies or to full-field flicker (saline: p = 0.267, DOI: p = 0.577) following DOI treatment (Figure 4E; saline: n = 100; DOI: n = 93). The observed changes in firing rate did not correlate with tuning properties or selectivity (not shown; saline preferred [pref] orientation [ori] stationary [stat]: r^2 = 0.012, pref ori moving [mv]: r^2 = 0.034, orientation selectivity index [OSI] stat: r^2 = 0.005, OSI mv: r^2 = 0.063; DOI: pref ori stat: r^2 = 0.0001; pref ori mv: r^2 = 0.0096; OSI stat: r^2 = 0.021; OSI mv: r^2 = 0.053).

To determine the similarity in receptive field structure before and after treatment, we calculated 2D correlation coefficients between raw spike-triggered average receptive fields (STAs) computed from pre- and post-recording sessions. We found no significant differences between the distributions of coefficients calculated from saline and DOI recording blocks (Figure 4F; two-sample t test: p = 0.348, n_{saline} = 28, n_{DOI} = 41). Thus, despite significant changes in temporal dynamics and spatial contextual modulation, basic tuning properties and receptive field structure of individual V1 neurons were unchanged after 5-HT_{2A}R activation.

DISCUSSION

Using widefield and two-photon calcium imaging and single-unit electrophysiology in awake mouse V1, we investigated how systemic administration of the hallucinogenic 5-HT_{2A}R agonist DOI affects cortical processing of visual information. We found reductions in response gain and surround suppression and altered temporal dynamics but no changes in basic tuning properties. Together, this study provides a systematic measurement of the effects of hallucinogenic 5-HT_{2A}R agonist administration on visual coding of cortical sensory neurons in awake animals.

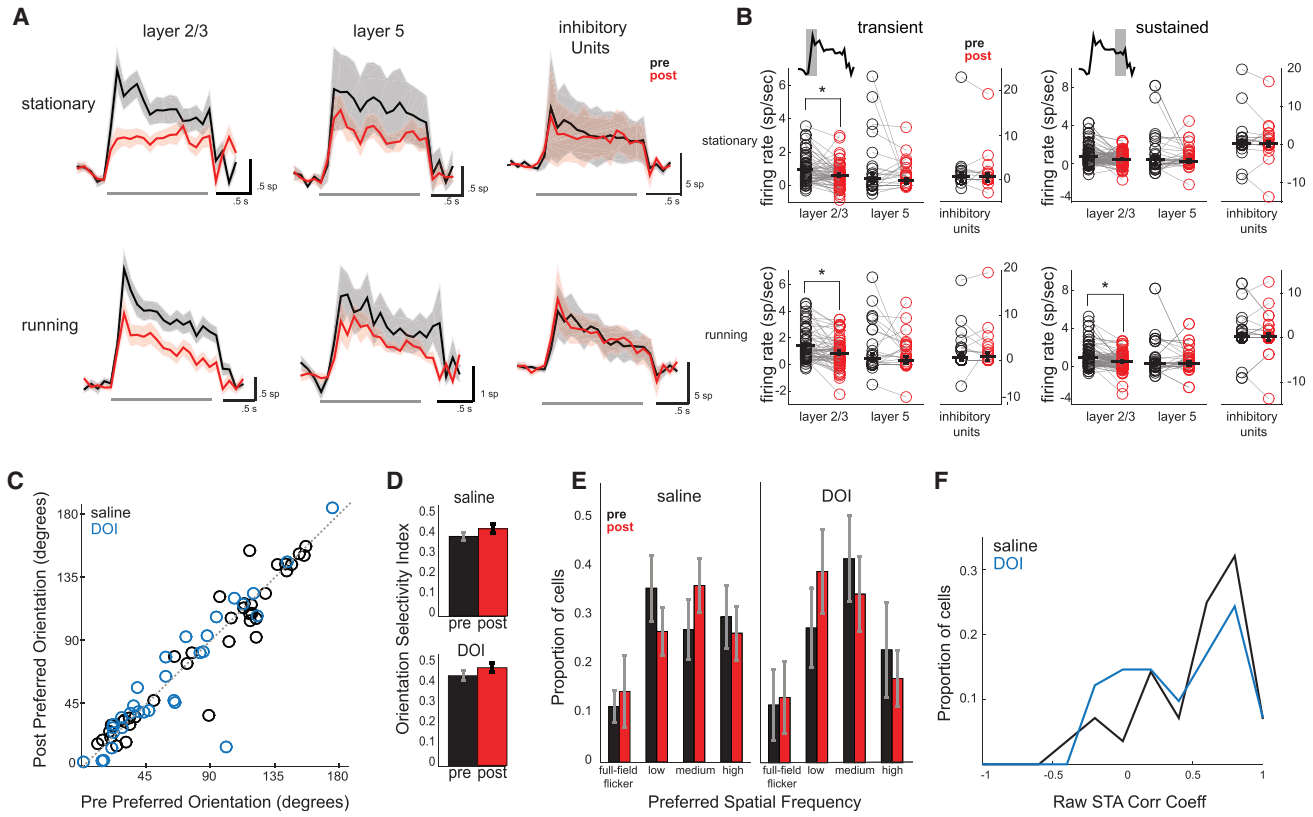

Figure 4. DOI Disrupts Temporal Dynamics in a Layer-Specific Manner but Maintains Tuning Properties

(A) Mean peristimulus time histograms ± SEM before (black) and after (red) administration of DOI across L2/3, L5, and inhibitory units during stationary and locomotive periods. Gray bars show stimulus period.

(B) Mean firing rate for each cell before or after DOI administration across transient and sustained components from PSTHs shown in (A). The transient component is defined as the first 500 ms after stimulus onset, and the sustained component is defined as the 500 ms preceding the stimulus offset (L2/3: n_{stat} = n = 37, n_{run} = 61; L5: n_{stat} = 13, n_{run} = 19; inh. n_{stat} = 7, n_{run} = 10).

(C) Preferred orientation of individual neurons before or after saline or DOI administration (n_{saline} = 37, n_{DOI} = 33).

(D) Average orientation selectivity index (OSI; circular variance) across populations of visually responsive cells before or after saline or DOI injection (n_{saline} = 100, n_{DOI} = 91).

(E) Proportion of visually responsive cells (>2 Hz) selective for preferred spatial frequencies before or after drug treatment (n_{saline} = 100, n_{DOI} = 93).

(F) Histograms of 2D correlation coefficients of raw spike triggered average receptive fields of all cells responsive above 2 Hz. A value of 1 represents STAs that did not change after saline or DOI administration (n_{saline} = 28, n_{DOI} = 41).

It remains to be determined whether the observed effects are due to action on 5-HT_{2A}Rs within V1 or elsewhere. Watakabe et al. (2009) administered DOI locally through microinfusions in V1 and also observed bidirectional firing rate modulation, suggesting that 5-HT_{2A}R activation in V1 is sufficient to drive neurophysiological changes consistent with systemic DOI administration. It is unknown, however, if local action of 5-HT_{2A}Rs in V1 alone is sufficient to drive perceptual changes. Furthermore, the circuit mechanisms by which these 5-HT_{2A}R-mediated changes occur are unclear. Evidence also suggests that other members of the 5-HT_2 receptor family are activated by DOI, albeit with significantly lower efficiency, and DOI is more selective for 5-HT_{2A}R than LSD (Knight et al., 2004). Given that our dose is comparable to most studies of 5-HT_{2A}R function (see STAR Methods for discussion), we do not expect this to be the case; however, we cannot rule out that 5-HT_{2B} or 5-HT_{2C} receptors contribute to our results. These issues will be important to address in future studies of psychedelic drug influence on sensory cortical processing.

5-HT_{2A}R Activation Reduces Sensory Drive

Models of hallucination suggest that reductions in bottom-up sensory drive can lead to a misinterpretation of sensory information. We observed reduced visually evoked widefield calcium activity, a measure of bulk activity in excitatory neurons, suggesting 5-HT_{2A}R activity reduces sensory drive in cortex. At the level of individual neurons, DOI administration bidirectionally modulated firing rates, but the overall effect was a decrease in V1 responses, which has also been observed in anesthetized primates and cats (Watakabe et al., 2009; Dray et al., 1980; Rose and Horn, 1977). Reduced sensory drive may lead to increased dependence on top-down expectations, leading to misinterpretation of sensory information, as hypothesized by current models of hallucination (Cassidy et al., 2018; Grossberg, 2000).

Previous *in vivo* studies have not discriminated between excitatory or inhibitory cell types or cortical layers in the context of 5-HT_{2A}R modulation of V1 response properties. Both excitatory and inhibitory populations showed bidirectional changes after DOI administration, though inhibitory neuron changes were not significant, possibly due to small sample size. Furthermore, 5-HT_{2A}R activation resulted in layer-specific modulation of excitatory neuron activity, decreasing evoked responses in L2/3. Given that subsets of excitatory and inhibitory neurons express 5-HT_{2A}Rs, with a majority in L5 (Weber and Andrade, 2010), it is possible that the directionality of DOI-induced change in a neuron's visual response is determined by whether it expresses 5-HT_{2A}R rather than its excitatory or inhibitory identity. Current evidence points toward increased excitability in 5-HT_{2A}R-expressing neurons (Avesar and Gulledge, 2012; Stephens et al., 2014), suggesting that non-expressing neurons, the majority of V1, may be suppressed via network mechanisms.

A recent study (Seillier et al., 2017) observed changes in visual responses after local iontophoresis of 5-HT into macaque V1 that were quite similar to those seen here, including a net decrease in response gain without change in selectivity, despite the fact that 5-HT itself acts on multiple receptor subtypes in cortex. Together, our findings suggest that at least in visual cortex the effect of 5-HT is dominated by the 2A subtype; however, future studies could further examine how different serotonin receptor subtypes contribute to modulation of sensory processing. Addressing these questions will require reliable genetic access to 5-HTR-family expressing neurons, which would also permit manipulations to determine the specific circuits mediating the effects observed here (Gong et al., 2007).

5-HT_{2A}R Activation Alters Visual Contextual Modulation in Excitatory V1 Neurons

Beyond CRF properties, contextual influences are critical components of visual processing. Lateral and top-down connections are thought to be key mediators of contextual processing, which is important for perceptual functions such as attention and figure-ground segregation. Disrupted contextual processing, including decreased visual surround suppression at the psychophysical and physiological levels, has been reported in patients with schizophrenia (Butler et al., 2008; Tibber et al., 2013; Zenger-Landolt and Heeger, 2003). Failure to appropriately incorporate contextual information could also underlie altered visual perception observed with psychedelic drugs. We found reduced surround suppression in V1 neurons resulting from decreased strength of driving and suppressive field coefficients after 5-HT_{2A}R activation, consistent with studies in patients with schizophrenia. This suggests these receptors may be important for adjusting the influence of context in visual cortical processing.

The magnitude of DOI-induced change in some measures was larger for trained than naive animals, including the amplitude of responses measured with widefield imaging and the suppressive field measured with two-photon imaging. Given that pupil diameter and time spent running did not consistently change after DOI administration (Figure S2), we do not anticipate changes seen here reflect solely changes in behavioral state or depth of field. Training on a visual task can result in a variety of changes in visual cortical processing, such as stimulus prediction or expectation, attention, stimulus encoding, and perceptual learning (for review, see Khan and Hofer, 2018). These learning-induced changes can be context specific and dependent on either bottom-up or top-down inputs. The various inputs to V1 that are modified by different learning paradigms could be differentially affected by neuromodulators, and untangling the logic of 5-HT_{2A}R modulation of specific V1 inputs may lend insight into the mechanisms of learning-induced changes in V1.

5-HT_{2A}R Activation Disrupts Temporal Dynamics of Visual Responses

DOI disrupted temporal dynamics at the population level, where we observed decreases in LFP power, and at the single-unit level, where we observed strong suppression of the transient onset response in L2/3 neurons. Previous studies suggest the transient component of visual responses are more weakly tuned than sustained responses (Ringach et al., 1997) and that transient responses may encode behaviorally relevant signals such as salience, novelty, or expectation (Homann et al., 2017; Fiser et al., 2016). Sustained responses may more accurately encode stimulus identity. We found that 5-HT_{2A}R activation differentially affected these response components in a cell-type- and layer-specific manner. Specifically, DOI altered transient responses in excitatory, but not inhibitory, L2/3 neurons, whereas sustained responses were unaffected. Given the relatively small effects of DOI on sustained relative to transient responses, along with the maintenance of feature selectivity in V1 neurons, these data suggest 5-HT_{2A}R activation does not disrupt stimulus encoding at the level of individual neurons but rather alters integration of top-down with bottom-up sensory information.

We also observed changes in temporal dynamics at the population level as a dramatic 5-HT_{2A}R-mediated decrease in visually evoked LFP power across V1 layers. Patients with schizophrenia (Uhlhaas and Singer, 2010; Moran and Hong, 2011) and subjects administered psychedelic drugs (Liechti, 2017) display reduced oscillatory power specifically in the gamma frequency band, which is associated with neuronal responses to visual stimuli (Liechti 2017; Sedley and Cunningham, 2013) and communication across neural populations through coordinated activity (Jia et al., 2013). Additionally, animal models of hallucination show reduced oscillatory synchronization across various brain areas (prefrontal cortex [PFC]: Wood et al., 2012; Celada et al., 2008; nucleus accumbens: Goda et al., 2013; hippocampus, striatum, and reticular formation: Dimpfel et al., 1989).

Implications for Models of Hallucination and Sensory Processing

Despite these DOI-mediated changes in V1 sensory drive and temporal dynamics, CRF tuning properties and stimulus encoding remained unchanged. This suggests that altered visual perception related to 5-HT_{2A}R function results not from changes in V1 stimulus encoding but from impaired downstream integration due to changes in gain and temporal dynamics. Consistent with these findings, many perceptual deficits in patients with schizophrenia are attributed to reduced gain of sensory responses (Butler et al., 2008; Phillips and Silverstein, 2013).

Understanding the action of 5-HT_{2A}Rs may provide insight into the general principles of cortical sensory processing, particularly given the potent impact of hallucinogenic 5-HT_{2A}R agonists on perception and cognition. There is increased urgency for understanding the neurophysiological effects of 5-HT_{2A}R modulation given the recent resurgence in use of psychedelic drugs in the treatment of mental health disorders (Johnson and Griffiths, 2017; Carhart-Harris and Goodwin, 2017). Our results provide a basis for investigating circuit-specific actions of these drugs in cortical function.

STAR★METHODS

Detailed methods are provided in the online version of this paper and include the following:

- KEY RESOURCES TABLE
- CONTACT FOR REAGENT AND RESOURCE SHARING
- EXPERIMENTAL MODEL AND SUBJECT DETAILS
- METHOD DETAILS
  - Surgical procedures
  - Experiments
  - Widefield Imaging
  - Two-photon imaging
  - Extracellular Multichannel Electrophysiology
- QUANTIFICATION AND STATISTICAL ANALYSIS
- DATA AND SOFTWARE AVAILABILITY

SUPPLEMENTAL INFORMATION

Supplemental Information can be found with this article online at https://doi.org/10.1016/j.celrep.2019.02.104.

ACKNOWLEDGMENTS

We thank Dr. David Fitzpatrick and Dr. Matt Smear for comments on the manuscript and members of the Niell lab for helpful discussions. This work was supported by NIH grants R01 EY023337 (C.M.N.), 2T32HD007348-26 (A.M.M.), and F32 EY027696-02 (P.R.L.P.)

AUTHOR CONTRIBUTIONS

A.M.M., P.R.L.P, and C.M.N. conceived of the project, designed experiments, analyzed data, and wrote the manuscript. A.M.M. performed electrophysiology experiments, P.R.L.P. performed two-photon imaging experiments, and A.M.M. and P.R.L.P. equally performed widefield imaging experiments.

DECLARATION OF INTERESTS

The authors declare no competing interests.

Received: July 28, 2018
Revised: November 6, 2018
Accepted: February 22, 2019
Published: March 26, 2019

REFERENCES

Aulakh, C.S., Hill, J.L., Yoney, H.T., and Murphy, D.L. (1992). Evidence for involvement of 5-HT_{1C} and 5-HT_2 receptors in the food intake suppressant effects of 1-(2,5-dimethyoxy-4-iodophenyl)-2-aminopropane (DOI). Psychopharmacology *109*, 444–448.

Avesar, D., and Gulledge, A.T. (2012). Selective serotonergic excitation of callosal projection neurons. Front. Neural Circuits *6*, 12.

Ayaz, A., Saleem, A.B., Schölvinck, M.L., and Carandini, M. (2013). Locomotion controls spatial integration in mouse visual cortex. Curr. Biol. *23*, 890–894.

Brainard, D.H. (1997). The psychophysics toolbox. Spat. Vis. *10*, 433–436.

Butler, P.D., Silverstein, S.M., and Dakin, S.C. (2008). Visual perception and its impairment in schizophrenia. Biol. Psychiatry *64*, 40–47.

Carhart-Harris, R.L., and Goodwin, G.M. (2017). The therapeutic potential of psychedelic drugs: past, present, and future. Neuropsychopharmacology *42*, 2105–2113.

Carhart-Harris, R.L., Muthukumaraswamy, S., Roseman, L., Kaelen, M., Droog, W., Murphy, K., Tagliazucchi, E., Schenberg, E.E., Nest, T., Orban, C., et al. (2016). Neural correlates of the LSD experience revealed by multimodal neuroimaging. Proc. Natl. Acad. Sci. USA *113*, 4853–4858.

Cassidy, C.M., Balsam, P.D., Weinstein, J.J., Rosengard, R.J., Slifstein, M., Daw, N.D., Abi-Dargham, A., and Horga, G. (2018). A perceptual inference mechanism for hallucinations linked to striatal dopamine. Curr. Biol. *28*, 503–514.e4.

Celada, P., Puig, M.V., Díaz-Mataix, L., and Artigas, F. (2008). The hallucinogen DOI reduces low-frequency oscillations in rat prefrontal cortex: reversal by antipsychotic drugs. Biol. Psychiatry *64*, 392–400.

Dimpfel, W., Spüler, M., and Nichols, D.E. (1989). Hallucinogenic and stimulatory amphetamine derivatives: fingerprinting DOM, DOI, DOB, MDMA, and MBDB by spectral analysis of brain field potentials in the freely moving rat (Tele-Stereo-EEG). Psychopharmacology (Berl.) *98*, 297–303.

Dombeck, D.A., Khabbaz, A.N., Collman, F., Adelman, T.L., and Tank, D.W. (2007). Imaging large-scale neural activity with cellular resolution in awake, mobile mice. Neuron *56*, 43–57.

Dray, A., Fox, P.C., Hilmy, M., and Somjen, G.G. (1980). The effects of LSD and some analogues on the responses of single cortical neurons of the cat to optical stimulation. Brain Res. *200*, 105–121.

Fiser, A., Mahringer, D., Oyibo, H.K., Petersen, A.V., Leinweber, M., and Keller, G.B. (2016). Experience-dependent spatial expectations in mouse visual cortex. Nat. Neurosci. *19*, 1658–1664.

Fox, P.C., and Dray, A. (1979). Iontophoresis of LSD: Effects on responses of single cortical neurons to visual stimulation. Brain Res. *161*, 167–172.

Freo, U., Holloway, H.W., Kalogeras, K., Rapoport, S.I., and Soncrant, T.T. (1992). Adrenalectomy or metyrapone-pretreatment abolishes cerebral metabolic responses to the serotonin agonist 1-(2,5-dimethoxy-4-iodophenyl)-2-aminopropoane (DOI) in the hippocampus. Brain Res. *586*, 256–264.

Garcia, E.E., Smith, R.L., and Sanders-Bush, E. (2007). Role of G(q)protein in behavioral effects of the hallucinogenic drug 1-(2,5-dimethoxy-4-iodophenyl)-2-aminopropane. Neuropharmacology *52*, 1671–1677.

Goda, S.A., Piasecka, J., Olszewski, M., Kasicki, S., and Hunt, M.J. (2013). Serotonergic hallucinogens differentially modify gamma and high frequency oscillations in the rat nucleus accumbens. Psychopharmacology (Berl.) *228*, 271–282.

Gong, S., Doughty, M., Harbaugh, C.R., Cummins, A., Hatten, M.E., Heintz, N., and Gerfen, C.R. (2007). Targeting Cre recombinase to specific neuron populations with bacterial artificial chromosome constructs. J. Neurosci. *27*, 9817–9823.

González-Maeso, J., Weisstaub, N.V., Zhou, M., Chan, P., Ivic, L., Ang, R., Lira, A., Bradley-Moore, M., Ge, Y., Zhou, Q., et al. (2007). Hallucinogens recruit specific cortical 5-HT(2A) receptor-mediated signaling pathways to affect behavior. Neuron *53*, 439–452.

Grossberg, S. (2000). How hallucinations may arise from brain mechanisms of learning, attention, and volition. J. Int. Neuropsychol. Soc. *6*, 583–592.

Hanks, J.B., and González-Maeso, J. (2013). Animal models of serotonergic psychedelics. ACS Chem. Neurosci. *4*, 33–42.

Harris, K.D., Henze, D.A., Csicsvari, J., Hirase, H., and Buzsáki, G. (2000). Accuracy of tetrode spike separation as determined by simultaneous intracellular and extracellular measurements. J. Neurophysiol. *84*, 401–414.

Hirota, J., and Shimizu, S. (2012). Routes of administration. In The Laboratory Mouse, Second Edition, H.J. Hedrick, ed. (Elsevier), pp. 709–725.

Homann, J., Koay, S.A., Glidden, A.M., Tank, D.W., and Berry, M.J., II. (2017). Predictive coding of novel versus familiar stimuli in the primary visual cortex. bioRxiv. https://doi.org/10.1101/197608.

Hoy, J.L., and Niell, C.M. (2015). Layer-specific refinement of visual cortex function after eye opening in the awake mouse. J. Neurosci. *35*, 3370–3383.

Jia, X., Tanabe, S., and Kohn, A. (2013). γ and the coordination of spiking activity in early visual cortex. Neuron *77*, 762–774.

Johnson, M.W., and Griffiths, R.R. (2017). Potential therapeutic effects of psilocybin. Neurotherapeutics *14*, 734–740.

Kalatsky, V.A., and Stryker, M.P. (2003). New paradigm for optical imaging: temporally encoded maps of intrinsic signal. Neuron *38*, 529–545.

Khan, A.G., and Hofer, S.B. (2018). Contextual signals in visual cortex. Curr. Opin. Neurobiol. *52*, 131–138.

Knight, A.R., Misra, A., Quirk, K., Benwell, K., Revell, D., Kennett, G., and Bickerdike, M. (2004). Pharmacological characterisation of the agonist radioligand binding site of 5-HT(2A), 5-HT(2B) and 5-HT(2C) receptors. Naunyn Schmiedebergs Arch. Pharmacol. *370*, 114–123.

Kometer, M., Schmidt, A., Jäncke, L., and Vollenweider, F.X. (2013). Activation of serotonin 2A receptors underlies the psilocybin-induced effects on α oscillations, N170 visual-evoked potentials, and visual hallucinations. J. Neurosci. *33*, 10544–10551.

Liechti, M.E. (2017). Modern Clinical Research on LSD. Neuropsychopharmacology *42*, 2114–2127.

Mayford, M., Bach, M.E., Huang, Y.Y., Wang, L., Hawkins, R.D., and Kandel, E.R. (1996). Control of memory formation through regulated expression of a CaMKII transgene. Science *274*, 1678–1683.

Mitra, P., and Bokil, H. (2007). Observed Brain Dynamics (Oxford University Press).

Mitra, P.P., and Pesaran, B. (1999). Analysis of dynamic brain imaging data. Biophys. J. *76*, 691–708.

Moran, L.V., and Hong, L.E. (2011). High vs low frequency neural oscillations in schizophrenia. Schizophr. Bull. *37*, 659–663.

Nichols, D.E. (2016). Psychedelics. Pharmacol. Rev. *68*, 264–355.

Niell, C.M., and Stryker, M.P. (2008). Highly selective receptive fields in mouse visual cortex. J. Neurosci. *28*, 7520–7536.

Niell, C.M., and Stryker, M.P. (2010). Modulation of visual responses by behavioral state in mouse visual cortex. Neuron *65*, 472–479.

Pelli, D.G. (1997). The VideoToolbox software for visual psychophysics: transforming numbers into movies. Spat. Vis. *10*, 437–442.

Phillips, W.A., and Silverstein, S.M. (2013). The coherent organization of mental life depends on mechanisms for context-sensitive gain-control that are impaired in schizophrenia. Front. Psychol. *4*, 307.

Pnevmatikakis, E.A., Soudry, D., Gao, Y., Machado, T.A., Merel, J., Pfau, D., Reardon, T., Mu, Y., Lacefield, C., Yang, W., et al. (2016). Simultaneous denoising, deconvolution, and demixing of calcium imaging data. Neuron *89*, 285–299.

Porter, W.P., Bitar, Y.M., Strandberg, J.D., and Charache, P.C. (1985). A comparison of subcutaneous and intraperitoneal oxytetracycline injection methods for control of infectious disease in the rat. Lab. Anim. *19*, 3–6.

Preller, K.H., Burt, J.B., Ji, J.L., Schleifer, C.H., Adkinson, B.D., Stämpfli, P., Seifritz, E., Repovs, G., Krystal, J.H., Murray, J.D., et al. (2018). Changes in global and thalamic brain connectivity in LSD-induced altered states of consciousness are attributable to the 5-HT2A receptor. eLife *7*, e35082.

Ringach, D.L., Hawken, M.J., and Shapley, R. (1997). Dynamics of orientation tuning in macaque primary visual cortex. Nature *387*, 281–284.

Rose, D., and Horn, G. (1977). Effects of LSD on the response of single units in cat visual cortex. Exp. Brain Res. *27*, 71–80.

Schindler, E.A.D., Dave, K.D., Smolock, E.M., Aloyo, V.J., and Harvey, J.A. (2012). Serotonergic and dopaminergic distinctions in the behavioral pharmacology of (±)-1-(2,5-dimethoxy-4-iodophenyl)-2-aminopropane (DOI) and lysergic acid diethylamide (LSD). Pharmacol. Biochem. Behav. *101*, 69–76.

Schmidt, C.J., Sorensen, S.M., Kehne, J.H., Carr, A.A., and Palfreyman, M.G. (1995). The role of 5-HT2A receptors in antipsychotic activity. Life Sci. *56*, 2209–2222.

Schmitzer-Torbert, N., Jackson, J., Henze, D., Harris, K., and Redish, A.D. (2005). Quantitative measures of cluster quality for use in extracellular recordings. Neuroscience *131*, 1–11.

Sedley, W., and Cunningham, M.O. (2013). Do cortical gamma oscillations promote or suppress perception? An under-asked question with an over-assumed answer. Front. Hum. Neurosci. *7*, 595.

Seillier, L., Lorenz, C., Kawaguchi, K., Ott, T., Nieder, A., Pourriahi, P., and Nienborg, H. (2017). Serotonin decreases the gain of visual responses in awake macaque V1. J. Neurosci. *37*, 11390–11405.

Shulgin, A., and Shulgin, A. (1991). Pihkal: A Chemical Love Story (Transform Press).

Sirota, A., Montgomery, S., Fujisawa, S., Isomura, Y., Zugaro, M., and Buzsáki, G. (2008). Entrainment of neocortical neurons and gamma oscillations by the hippocampal theta rhythm. Neuron *60*, 683–697.

Stephens, E.K., Avesar, D., and Gulledge, A.T. (2014). Activity-dependent serotonergic excitation of callosal projection neurons in the mouse prefrontal cortex. Front. Neural Circuits *8*, 97.

Tibber, M.S., Anderson, E.J., Bobin, T., Antonova, E., Seabright, A., Wright, B., Carlin, P., Shergill, S.S., and Dakin, S.C. (2013). Visual surround suppression in schizophrenia. Front. Psychol. *4*, 88.

Turner, P.V., Pekow, C., Vasbinder, M.A., and Brabb, T. (2011). Administration of substances to laboratory animals: equipment considerations, vehicle selection, and solute preparation. J. Am. Assoc. Lab. Anim. Sci. *50*, 614–627.

Uhlhaas, P.J., and Singer, W. (2010). Abnormal neural oscillations and synchrony in schizophrenia. Nat. Rev. Neurosci. *11*, 100–113.

Vollenweider, F.X., Vollenweider-Scherpenhuyzen, M.F., Bäbler, A., Vogel, H., and Hell, D. (1998). Psilocybin induces schizophrenia-like psychosis in humans via a serotonin-2 agonist action. Neuroreport *9*, 3897–3902.

Watakabe, A., Komatsu, Y., Sadakane, O., Shimegi, S., Takahata, T., Higo, N., Tochitani, S., Hashikawa, T., Naito, T., Osaki, H., et al. (2009). Enriched expression of serotonin 1B and 2A receptor genes in macaque visual cortex and their bidirectional modulatory effects on neuronal responses. Cereb. Cortex *19*, 1915–1928.

Weber, E.T., and Andrade, R. (2010). Htr2a gene and 5-HT(2A) receptor expression in the cerebral cortex studied using genetically modified mice. Front. Neurosci. *4*, 36.

Wekselblatt, J.B., Flister, E.D., Piscopo, D.M., and Niell, C.M. (2016). Large-scale imaging of cortical dynamics during sensory perception and behavior. J. Neurophysiol. *115*, 2852–2866.

Wood, J., Kim, Y., and Moghaddam, B. (2012). Disruption of prefrontal cortex large scale neuronal activity by different classes of psychotomimetic drugs. J. Neurosci. *32*, 3022–3031.

Zenger-Landolt, B., and Heeger, D.J. (2003). Response suppression in v1 agrees with psychophysics of surround masking. J. Neurosci. *23*, 6884–6893.

STAR★METHODS

KEY RESOURCES TABLE

REAGENT or RESOURCE	SOURCE	IDENTIFIER
Experimental Models: Organisms/Strains		
Mouse: C57 Bl/6J	JAX	JAX: 000664
Mouse: CaMKII-tTA:tetO-GCaMP6s	Mayford et al., 1996; Wekselblatt et al., 2016	JAX: 007004 and 024742
Chemicals, Peptides, and Recombinant Proteins		
(±)-DOI hydrochloride	Sigma-Aldrich	Cat#: D101-10MG
Software and Algorithms		
2-p Cell Extraction	Pnevmatikakis et al., 2016	N/A

CONTACT FOR REAGENT AND RESOURCE SHARING

Further information and requests for resources and reagents should be directed to and will be fulfilled by the Lead Contact, Cristopher Niell (cniell@uoregon.edu).

EXPERIMENTAL MODEL AND SUBJECT DETAILS

Animals: All procedures were conducted in accordance with the guidelines of the National Institutes of Health and were approved by the University of Oregon Institutional Animal Care and Use Committee. Two- to eight-month old adult mice [C57BL/6J for electrophysiology, CaMKII-tTA:tetO-GCaMP6s (Jackson Laboratories stock numbers 007004 and 024742) for imaging (Mayford et al., 1996; Wekselblatt et al., 2016)] were initially implanted with a steel headplate over primary visual cortex to allow for head-fixation during electrophysiology (Niell and Stryker, 2008) or imaging (Wekselblatt et al., 2016) experiments. In total, 26 male and 39 female mice were used for this study. Animals were handled by the experimenter for several days before surgical procedures, and subsequently habituated to the spherical treadmill for several days before experiments. Some mice in imaging experiments were previously trained on a two-alternative forced choice task, where they were water restricted and given water rewards based on leftward or rightward movements of the spherical treadmill during luminance discrimination and orientation/spatial discrimination of a grating patch (for details, see Wekselblatt et al., 2016). The grating patches presented during passive viewing in this study were similar in quality (45 deg, 0.16 cycles/degree for behavior, see below for passive parameters) but presented in a different location in visual space compared to the previous behavioral training. These mice were not water restricted during the current experiments, and imaging experiments performed under identical conditions as naive groups.

METHOD DETAILS

Surgical procedures

Animals were anesthetized with isoflurane (3% induction, 1.5%–2% maintenance, in O_2) and body temperature was maintained at 37.5°C using a feedback-controlled heating pad. Fascia was cleared from the surface of the skull following scalp incision and a custom steel headplate containing a circular well was attached to the skull using Vetbond (3M) and dental acrylic. The headplate well was centered over V1 (2.5-3 mm lateral of the midline and 1 mm anterior of Lambda). Carprofen (10 mg/kg) and lactated Ringer's solution were administered subcutaneously, and animals were monitored for three days following surgery.

For widefield imaging, a protective layer of cyanoacrylate adhesive (Loctite) was applied to the skull within the headplate well (10 mm diameter) during headplate attachment. For two-photon experiments, a second surgery was performed at least 3 days after headplate attachment, whereby a section of skull ~5 mm in diameter was removed via dental drill, artificial dura (Dow-Corning 3-4680 Silicone Gel) was applied in the craniotomy, and a 5 mm glass coverslip was glued into place over the craniotomy. Antibiotics (cefazolin, 10 mg/kg) were administered in the week surrounding the surgery, and an anti-inflammatory (dexamethasone, 10 mg/kg) was administered 18h and 2h prior to surgery to prevent brain swelling.

For electrophysiology experiments, at least two days following headplate attachment a craniotomy (1 mm diameter) was made the night before or several hours prior to the recording session. The cortical surface was covered with a layer of 1.5% agarose in 0.9% saline and a layer of Kwik-Sil (WPI) to prevent drying and provide structural support.

Experiments

Mice were head-fixed above a spherical treadmill and locomotion was measured via an optical mouse placed on the side of the spherical treadmill using a custom MATLAB script. Visual stimuli were generated in MATLAB using the Psychophysics toolbox extensions (Brainard 1997; Pelli 1997), and presented on gamma-corrected LED monitors oriented tangentially 20-25 cm from the contralateral eye (plus ipsilateral eye for widefield retinotopic mapping). Saline (0.9% NaCl) or DOI (Sigma, 10 mg/kg in saline) was then administered subcutaneously, and visual responses to the same stimulus set (presented in reverse order) were recorded again after a waiting period of 15-20 min. Mice were monitored for front paw stereotypy, which DOI reliably induced within 5-7 min following injection.

This dose of 10 mg/kg was chosen based on standards in the literature, which range from 1-10 mg/kg intraperitoneal (Freo et al., 1992; Aulakh et al., 1992; Garcia et al., 2007; González-Maeso et al., 2007). Subcutaneous injection was used rather than intraperitoneal to prevent having to remove the animal from the head-fixed setup between pre and post stimulus presentations. We estimate that our effective dose is approximately equivalent to 2.5 mg/kg intraperitoneal based on previous comparisons of the two injection methods, where serum levels tend to rise more slowly and peak at significantly lower concentrations after subcutaneous injection (Porter et al., 1985; Turner et al., 2011; Turner et al., 2011; Hirota and Shimizu, 2012). Previous work revealed LSD elicited head bob behavior in rabbits occurs independent of the route of administration (Schindler et al., 2012). However, to confirm that we were not using an excessively high dose, we tested a lower dose in a subset of widefield experiments (2 mg/kg subcutaneous) and saw no significant change in response amplitude relative to baseline (see Figure S1).

Widefield Imaging

A widefield microscope (Scimedia, Inc.) equipped with a sCMOS camera (PCO, 10 Hz acquisition) was used to measure GCaMP6s signal though the skull during blue LED excitation (Luxeon Rebel 470 nm, 0.1 mW/mm^2 at the sample). In a subset of experiments, a green LED (Luxeon Rebel 530 nm, 0.1 mW/mm^2 at the sample) was used for excitation every four frames to measure hemodynamic signals, which were subtracted from the blue frames (Wekselblatt et al., 2016). The change in fluorescence relative to baseline ($\Delta F/F$) was calculated for each pixel individually using its mean value as F. Visual areas were first mapped using a topographic stimulus consisting of a bar of 1/f noise sweeping in either azimuth or elevation, and the amplitude and phase of the Fourier component of the $\Delta F/F$ signal were calculated at the stimulus frequency (0.1 Hz), which were later used to align sessions across animals (Kalatsky and Stryker, 2003). Vertical and horizontal stationary grating patches (0.16 cpd, 30 deg) were presented to the right eye with 1 s duration and 1 s inter-stimulus interval. For each animal, a central point in V1 corresponding to the approximate response peak was selected, and the pixels around this point in a 5 X 5 region were averaged to create $\Delta F/F$ traces. To analyze spatial spread of responses, an elliptical meshgrid was generated around this central point, with a 2:1 ratio of the major:minor axes aligned in the anteroposterior:mediolateral dimensions to account for cortical magnification factor, and the points along this meshgrid radiating out from the center were averaged along these concentric ellipses to create an average $\Delta F/F$ for a given distance from the center point along the minor axis of the ellipse. Normalized $\Delta F/F$ change was calculated as (post-pre)/mean(post,pre).

Two-photon imaging

A two-photon microscope (Neurolabware, 16X Nikon CFI75 LWD objective) was used to measure GCaMP6s signal through the cranial window at 920 nm laser excitation (Mai-Tai, Spectra-Physics). $\sim$800 μm by 800 μm frames were acquired at 10 Hz using Scanbox software. Visual areas were first mapped using widefield imaging (described above), then V1 was targeted and the stimulus screen and field of view were adjusted to center the visual response. A mapping stimulus (see widefield imaging methods) was first used to measure spatial receptive fields, followed by a period of darkness (5 min) to measure spontaneous activity. Then a $\sim$22 min stimulus was shown to measure surround suppression, which consisted of binarized grating patches at various sizes (5, 10, 20, 30, 40, and 50 deg of visual field), spatial frequencies (0.04, 0.16 cycles/deg), and orientations (0, 90°) at a 2 Hz temporal frequency and full contrast, with 0.5 s duration and 0.5 s inter-stimulus interval.

Cell footprints were extracted using constrained nonnegative matrix factorization, with a spatially homogeneous neuropil response factored out (Pnevmatikakis et al., 2016). $\Delta F/F$ was calculated for all pixels using the 10th percentile as F, and then traces for all cells were deconvolved using constrained foopsi. Data for each specific stimulus were then analyzed using custom MATLAB scripts. For surround suppression data, $\Delta F/F$ within each inter-trial-interval was averaged and subtracted from the ensuing trial, and the $\Delta F/F$ traces during blank stimuli (mean luminance gray identical to inter-trial-interval) were averaged across the experiment and subtracted from all trials (separately for stationary and running trials). Only neurons whose somata were within the region of neuropil activated by the 10 deg stimulus were included in the analysis, constrained within an elliptical region with a 2:1 major:minor axis ratio along the anteroposterior:mediolateral dimensions to account for cortical magnification factor, with a manual rotational offset and overall size chosen to closely match each individual animal's response pattern. Within this region, only neurons with responses to any one of the stimulus types (combination of size, spatial frequency, orientation) greater than 10% $\Delta F/F$ for both pre and post drug injection were included in analyses. For all two-photon group analyses, averages were taken across cells (within animal) and these values were then used to calculate group mean/standard error. For surround suppression experiments, a divisive normalization model

(Ayaz et al., 2013) was used to fit the data for pre and post injection periods separately, then all variables except R_D and R_S were constrained as the average of pre/post values, and the fits were run again. The equation fit to each animal's size tuning curve was:

$$R(d) = \frac{RD * \left(\text{erf}\left(\frac{d}{sqrt(2) * \sigma D}\right)\right)^m}{1 + RS * \left(\text{erf}\left(\frac{d}{sqrt(2) * \sigma S}\right)\right)^m}$$

where R_D and R_S are the strengths of the driving and suppressive fields, σ_D and σ_S are the extents of the driving and suppressive fields, m is an exponent, d is the diameter of the stimulus, and erf is the error function. The coefficient of determination for each group was: saline naive r^2 = 0.939, saline trained r^2 = 0.928, DOI naive r^2 = 0.867, DOI trained r^2 = 0.941, and there was no significant difference between pre and post fit r^2 for any group (paired t test). Suppression index was calculated as $(R_{MAX} - R_{50d})/(R_{MAX} + R_{50d})$ where R_{MAX} is the largest response across all sizes, and R_{50d} is the response to the largest stimulus (50 deg). Normalized change for R_D, R_S, and suppression index was calculated as (post-pre)/mean(post,pre).

Extracellular Multichannel Electrophysiology

Multisite silicon probes (NeuroNexus, A2x32-5mm25-200-177) coated with a small amount of the lipophilic dye DiO (Invitrogen) were inserted through the overlaying agarose and into monocular V1 using a microdrive (Siskiyou Designs). Electrode penetrations were done over the course of 30 min – 1 h and the probe was allowed to settle in its final position for at least 30 min before data collection began. Hand-mapped receptive fields were used to approximately center the screen position on receptive field centers. Contrast-modulated noise movies (Gaussian 1/f) were presented and spike-triggered averaging (STA) was utilized to estimate spatial receptive fields as in Niell and Stryker (2008). Full-field drifting sinusoidal gratings were presented at twelve evenly spaced directions of motion, six spatial frequencies (0.01, 0.02, 0.04, 0.08, 0.16, and 0.32 cpd), and full-field flicker (0 cpd) with temporal frequency of 2 Hz. Stimulus presentations were randomly interleaved for 1.5 s duration, with 1 s inter-stimulus interval. To estimate spontaneous firing rate, a gray blank condition (mean luminance) was also presented. For darkness recordings, the computer monitor was turned off and other sources of light in the room were covered.

At the end of the experiment, animals were euthanized by deep anesthesia and cervical dislocation. Following removal, brains were immersed in 4% PFA (Electron Microscopy Sciences) in PBS at 4°C. 100 μm coronal sections were cut with a vibratome and mounted using Vectashield with DAPI (Vector Laboratories) then imaged on a Zeiss Axio Imager 2 to determine the depth of electrode penetrations. Each site along the electrode was given a layer assignment based on its position on the probe relative to the depth of the probe tip and geometry of the penetration angle. In addition to histology, current source density was also used to identify cortical layers in neural recordings (Hoy and Niell, 2015).

Data acquisition was performed as described by Niell and Stryker (2008). Signals were acquired using a System 3 workstation (Tucker-Davis Technologies) and analyzed with custom software in MATLAB (MathWorks). Extracellular signals were filtered from 0.7 to 7 kHz and sampled at 25 kHz. We detected spiking events on-line by voltage threshold crossing, and a 1 ms waveform sample on four adjacent recording sites was acquired, creating a virtual tetrode. Single-unit clustering and spike waveform analyses were performed using a combination of custom software in MATLAB and Klusta-Kwik (Harris et al., 2000), as described previously (Niell and Stryker, 2008). Quality of unit separation was based on a clear refractory period of less than 0.01% of spikes within a 1 ms inter-spike interval and by the computed *L* ratio (Schmitzer-Torbert et al., 2005). Units were also checked for stability by confirming that their peak amplitude remained consistent over the course of the recording session. Units that were found by histology to be outside of V1 were excluded from subsequent analysis.

Movement signals from the optical mouse were acquired at up to 300 Hz and integrated at 100 ms intervals (Mx310; Logitech), as originally described by Niell and Stryker (2010). By using these measurements, we calculated animals' mean speed for every stimulus presentation. Trials with mean speed above 0.5 cm/s were considered movement trials.

For LFP analysis, the extracellular signal was filtered from 1 to 300 Hz and sampled at 1.5 kHz. The power spectrum was computed using multi-taper estimation in MATLAB with the Chronux package (Mitra and Pesaran, 1999; Mitra and Bokil, 2007), with a sliding window and three to five tapers. Spectra were normalized for presentation by applying a 1/f correction (Sirota et al., 2008). Traces of individual experiments were normalized to the range of either the pre or post recording block across all experiments before averaging.

Units were classified as narrow or broad spiking based on properties of their average waveforms at the electrode site with largest amplitude. As detailed in Niell and Stryker (2008), two parameters—(1) height of the positive peak relative to the initial negative trough and (2) time from the minimum of the initial trough to maximum of the following peak—were sufficient to generate two linearly separable clusters corresponding to narrow spiking (putative inhibitory) and broad-spiking (putative excitatory) neurons. These clusters were separated using K-means.

Average evoked firing rate was calculated following a baseline subtraction of the spontaneous rate during 1 s inter-stimulus intervals. Modulation indices were calculated for evoked (1 Hz threshold) and spontaneous (0.5 Hz threshold) rates where MI = $(R_{post}-R_{pre})/(R_{post}+R_{pre})$. Peri-stimulus time histograms were calculated using 100 ms time bins over the 1.5 s duration of

each stimulus presentation and 1 s ISI. Visually responsive units included in the analysis were defined as units with an average firing rate above 2 spikes/s after baseline subtraction for either pre or post recording blocks.

We calculated preferred angle of orientation by finding the stimulus orientation that elicited the peak response for each cell on average, regardless of spatial frequency. The OSI was calculated as the depth of modulation from the preferred orientation to its orthogonal orientation $\theta_{ortho} = \theta_{pref} + \pi/2$, as $(R_{pref} - R_{ortho})/(R_{pref} + R_{ortho})$. Preferred spatial frequency was determined by finding the spatial frequency that elicited the largest response, on average. We used STAs of individual units recorded before and after drug administration to calculate 2-D correlation coefficients as a measure of similarity of receptive field structure.

QUANTIFICATION AND STATISTICAL ANALYSIS

Two-tailed paired t tests or Wilcoxon Rank sum tests were used to compare data before versus after drug administration. For comparisons between saline and DOI, two-sample tests such as Kolmogorov-Smirnov or two-sample two-tailed t tests were used. For comparison of trained and naive saline and DOI groups, Kruskal-Wallis and post hoc Tukey-Kramer tests were used. Significance was defined as $p < 0.05$, and in the case of multiple comparisons a Bonferroni correction was implemented.

DATA AND SOFTWARE AVAILABILITY

Datasets and custom MATLAB codes used for analysis are available upon request to Lead Contact, Cristopher Niell (cniell@uoregon.edu).

Cell Reports, Volume *26*

Supplemental Information

A Hallucinogenic Serotonin-2A Receptor Agonist Reduces Visual Response Gain and Alters Temporal Dynamics in Mouse V1

Angie M. Michaiel, Philip R.L. Parker, and Cristopher M. Niell

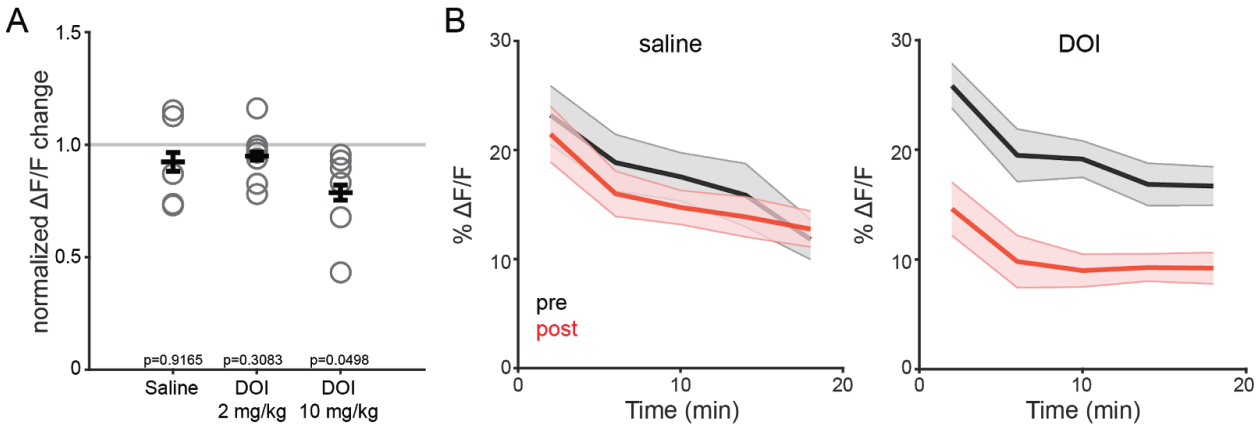

Figure S1: Dosage effects and kinetics of DOI-induced changes in V1 activity. Related to all main text Figures. A) Comparison of changes to visually evoked widefield responses after drug administration across groups of naive animals (as in Figure 1D-F). Open circles are individual animals, bars are mean ± SEM. A value of 1 represents no change, p-values are two-tailed paired t-test for pre vs. post within group. B) Time course of visually-evoked activity from two-photon experiments. The same stimulus set is repeat before (black) and after (red) drug injection. Values are mean ± SEM, n=animals/cells: saline = 22/413, DOI = 17/359.

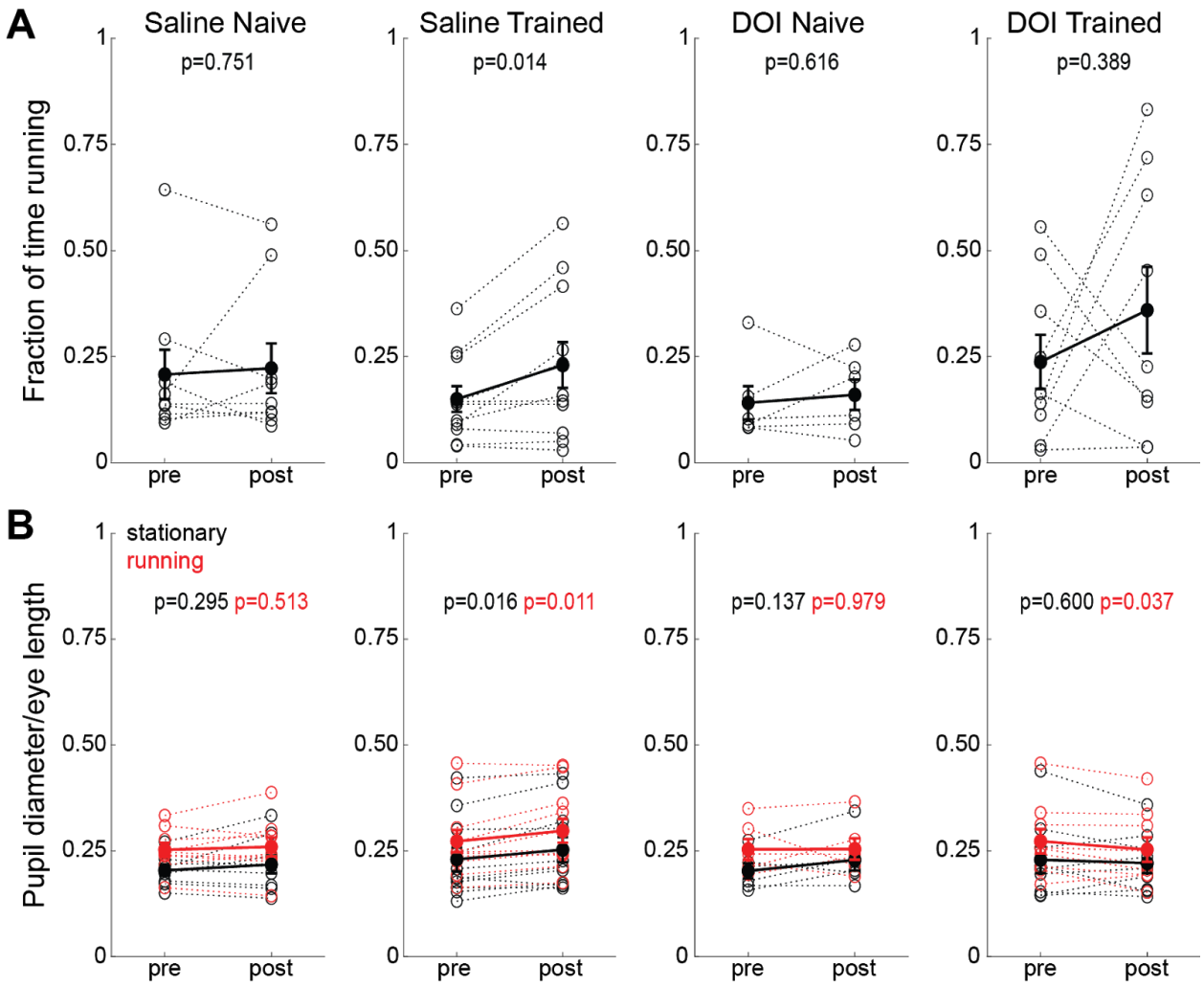

Figure S2: Baseline and post-drug measures relating to behavioral state. Related to Figure 2. A) Total fraction of experiment time spent running before (pre) and after (post) administration of saline or DOI for each group during two-photon imaging. Open circles connected by dotted lines represent individual animals and closed circles connected by thick lines with error bars are group mean ± SEM. Significance from paired t-tests are reported above each group plot. B) Average pupil diameter normalized to length of the animal's eye before and after drug administration. Black data represent stationary and red represent running periods. Open circles connected by dotted lines represent individual animals and closed circles connected by thick lines with error bars are group mean ± SEM.

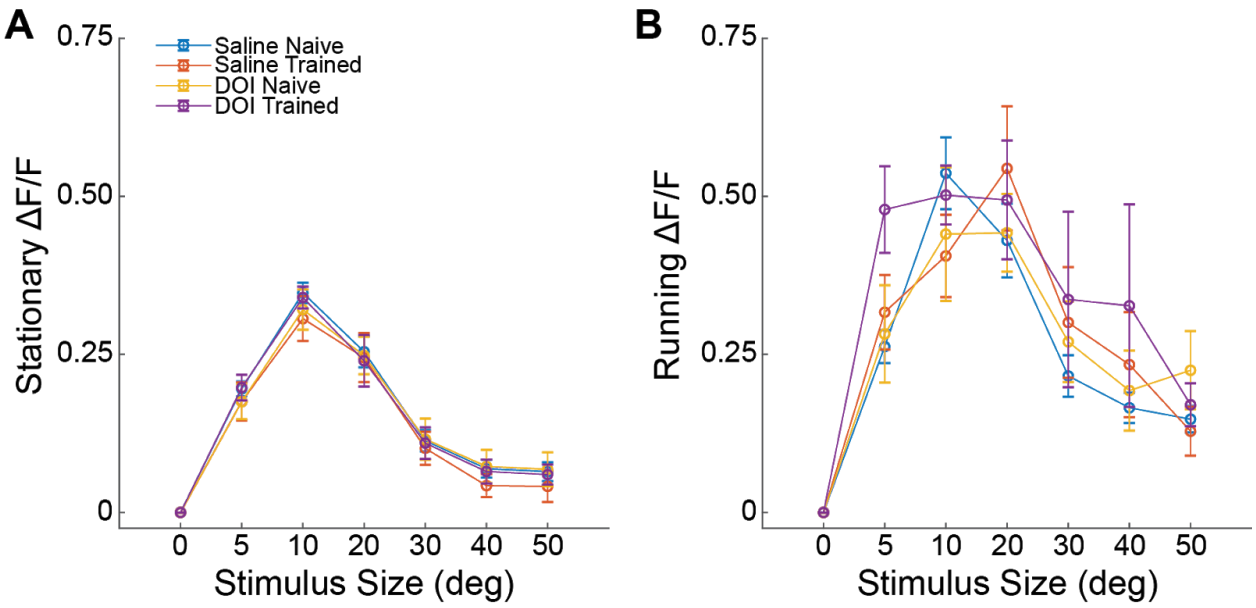

Figure S3: Comparison of baseline response magnitudes across experimental groups. Related to Figure 2. Size tuning curves showing baseline response magnitudes (before drug application) of all four groups for A) stationary, and B) running periods ($p = 0.619$ stationary, $p = 0.939$ running, Kruskal-Wallis). Open circles are group means and error bars are SEM.